Enhanced Tracking for Nanopositioning Systems Using Feedforward/Feedback Multivariable Control Design

Mohamed Kara-Mohamed, William P. Heath, and Alexander Lanzon

Abstract—This paper proposes a systematic synthesis methodology for a combined feedforward/feedback architecture to control multiple-input, multiple-output nanopositioning systems. Coprime factorization of the open loop model is used to design the reference and feedforward filters of the proposed control scheme to achieve enhanced tracking, eliminate the limitation of the feedback on tracking performance, and increase the bandwidth of the closed-loop system. Two types of coprime factorization, namely inner–outer factorization and normalized coprime factorization are discussed. A case study based on hardware experiment is presented to analyze the proposed control architecture and demonstrate its superiority over feedback-only control. In addition to the no-load case, the performance of the system is also tested with loads on the nanopositioning stage.

Index Terms—Feedback, feedforward, multivariable control design, nanopositioning, tracking.

I. INTRODUCTION

NANOPOSITIONING stages are used in a wide range of nanosciences and nanotechnologies, for example, atomic force microscopes (AFMs), scanning tunneling microscopes, lithography tools, and molecular biology [1]. These stages are typically flexible structures driven by piezoelectric actuators with the position measured by capacitive sensors. Piezoelectric actuators produce large forces with frictionless motion which makes these devices ideal for high-speed and high-resolution positioning [2]. However, control of nanopositioning stages is technically challenging [1], [3]. The dynamic control is limited by several nonlinearities, such as hysteresis and creep, and many lightly damped resonances whose frequencies vary with load [1], [4]. Robust feedback control theory, such as negative-imaginary systems theory [5], [6] in the context of nanopositioning control, can be used to desensitize the closed loop against some of these uncertainties and disturbances.

A. Limitations of Feedback Control

Tracking control of nanopositioning systems can be achieved using feedback schemes. However, for such lightly damped systems, controllers are typically designed with low bandwidth to preserve robustness [3], [7] and therefore the operating bandwidth of the closed loop is limited. Moreover, applications have recently emerged with high demands of increasing bandwidth and load requirements [1], [8]. In response to these requirements and to overcome the challenging problem of the bandwidth limitation, several feedback controllers have been introduced in the literature attempting to damp the resonant peaks and increase the bandwidth (see for example [3], [9]–[12] and references therein). However, these methods are still has the well-known fundamental limitations of feedback [13]. Six fixed-structure feedback-based damping control techniques have been analyzed and experimentally compared in [14] with a conclusion that the performance is fairly similar among these schemes. In practice, the maximum closed-loop bandwidth is less than 2% of the first resonance frequency when single degree-of-freedom feedback-only control is used [3].

B. Feedforward Control

The role of feedforward control in nanopositioning applications is reviewed in [8]. Inversion-based feedforward controllers are popular as solutions for high speed scanning. However, feedforward controllers lack the necessary robustness when nonlinearities and model uncertainties exist, which is inevitable in nanopositioning stages. Furthermore, if a significant change of the resonant peak occurs, feedforward control becomes infeasible [3]. Existence of nonminimum phase zeros represents another limitation for the implementation of inversion-based feedforward control. Therefore, the implementation of inversion-based feedforward controllers for nanopositioning stages can only considered for limited applications where the resonant frequencies are stable or the controller can be recalibrated online or offline [10], [15], [16]. Bounds on the uncertainty of the plant dynamics for the implementation of inversion-based feedforward control in nanopositioning systems are discussed in [17].

C. Feedforward/Feedback Control

In control theory, methods to relieve the fundamental limitations imposed by single degree-of-freedom control

while preserving the robustness properties include two degree-of-freedom control or more precisely combined feedforward/feedback (Ff/Fb) control. Two degree-of-freedom controllers possess advantages over one degree-of-freedom ones [18]. Ideally, the feedforward filter is designed via inversion of the nominal open loop model to enhance the tracking performance while the feedback controller maintains the robustness of the system against disturbances and uncertainties.

For nanopositioning systems, a combination of feedforward and feedback control can be considered to improve the tracking performance, increase the bandwidth, and retain the robustness of the closed-loop system [19]. For certain choices of reference trajectories, the feedforward filter is used for input-shaping to minimize excitation of the vibration modes. For instance, in [20], the feedforward/feedback structure is used to shape certain types of reference signals in an attempt to improve the positioning accuracy. If the type of the reference trajectory is not available, then the feedforward filter is designed via inverting the dynamics of the system. Two types of feedforward/feedback control based on the inversion approach, that is, inverting either the model of the open loop system or the model of the closed-loop system, are discussed in [21] with a concluding remark that the open loop inversion method is more useful for better positioning performance. Eleftheriou and Moheimani [22] have discussed the role of the feedforward/feedback control design in improving the bandwidth of the closed-loop system without compromising the robustness properties.

On the other hand, conventional Ff/Fb control inherits the synthesis challenges of the feedforward control for nonminimum phase systems, where the inversion of nonminimum phase systems produces internally unstable systems. This limitation of the conventional Ff/Fb for nanopositioning systems has been discussed in [22]. Moreover, the discrepancy between the system dynamics and the fitted model affects the tracking performance and limits the advantages of the design. Given these factors, Ff/Fb control schemes are poorly explored in depth for nanopositioning stages. Pao *et al.* [23] have combined a PI feedback controller with a model-inverse-based feedforward filter for an AFM application, yet the results are based on simulation study only and for a decoupled system. In [22], a combined Ff/Fb control is proposed where the design of the feedback controller is associated with the design of the feedforward filter via one cost function, a minimization problem and LMI.

D. SISO Stages Versus MIMO Stages

The literature of nanopositioning systems is rich with SISO control design associated with single degree-of-freedom feedback structure. Multiaxis stages are commonly considered as decoupled systems where cross-coupling between channels is ignored (see [1], [24], [25], and references therein). This trend is due to the fact that coupling in flexible structures becomes negligible when operating at very low speed [26]. However, the coupling becomes more significant as the operational speed increases. The decoupling assumption becomes

Fig. 1. Ff/Fb control structure to decouple the tracking performance from the feedback loop.

questionable when the operating bandwidth is close to the first resonant peak.

E. Contribution of the Paper

System factorization in control theory has played a crucial role for improving the design of combined Ff/Fb control structures to achieve enhanced tracking [27]. Special forms of coprime factorization can be utilized to enable the design of the feedforward filter in case of nonminimum phase zeros to enhance the tracking performance of the system. Ff/Fb structures based on coprime factorization have not been previously investigated for nanopositioning systems. In this paper, we propose a systematic Ff/Fb control method for multiple-input, multiple-output (MIMO) nanopositioning stages based on a specific two degree-of-freedom structure. The proposed structure is a special case of a class discussed in [28] and [29], which in turn builds on [27] and [30]. Coprime factorization of the nominal open loop stage's model is used to design the reference filter and the feedforward filter of the architecture, and hence overcome the problem of inverting nonminimum phase zeros. The proposed Ff/Fb structure increases the bandwidth of the closed loop while preserving the robustness of the system. It separates completely the nominal tracking performance of the system from the robustness consideration of the feedback loop. In the nominal case, the feedback controller has no effect on the tracking performance of the system. The feedback controller can be designed using any well-known method in the literature and in this paper it is synthesized using the $\mathcal{H}_\infty$ loop-shaping design method. A two-axis commercial stage is used to test the proposed control method and analyze its effectiveness.

The paper begins with the design methodology for enhanced tracking by using Ff/Fb structure as described in Section II. The effectiveness of the proposed methodology is demonstrated via a case study on the commercial nanopositioning stage NPS-XY-100A from Queensgate, Inc. in Section III. A summary of the results along with concluding remarks is provided in Section IV.

II. DESIGN METHODOLOGY FOR ENHANCED TRACKING

Consider the control structure proposed in [28] and [29]. The same structure is shown in Fig. 1 with conventional diagram flow for ease of understanding from an engineering point of view.

Let G be a continuous LTI transfer function matrix that represents the model of the nanopositioning system and can be factorized as $G = NM^{-1}$, where N and M are right coprime

factors. Let C_b be a feedback controller that is designed by any existing method. The external filters X, Y, and F are designed to be stable so that the reference injection and the control action injection are bounded signals.

The transfer function matrix from the reference command vector r to the output position vector y is given by

$$T_{\mathrm{ry}} = G(I + C_b G)^{-1}(C_b Y + X)F. \qquad (1)$$

It is also important to consider the transfer function matrix from the reference vector r to the system input vector u as this is a measure for control energy and actuator effort to achieve the required tracking performance. This transfer function from r to u is given by

$$T_{\mathrm{ru}} = (I + C_b G)^{-1}(C_b Y + X)F. \qquad (2)$$

Using the coprime factors M and N to design the feedforward and reference filters such that $X = M$ and $Y = N$ yields $T_{\mathrm{ry}} = NF$ and $T_{\mathrm{ru}} = MF$. Therefore, it can be seen that this structure separates the nominal set-point tracking design from the robustness feedback design of the closed-loop system. The nominal output-tracking performance is only constrained by the Right-Half-Plane (RHP) zeros of the stage and the nominal control action is only constrained by the RHP poles of the stage. No limitation results from the RHP zeros or poles of the feedback controller C_b and no limitation results from the RHP poles of the stage on the tracking performance. Furthermore, as X and Y are in $\mathcal{RH}_\infty$, the feedback loop shown in Fig. 1 between G and C_b can be considered separately. Hence, the robustness and the nominal tracking performance of the system can be designed independently. This can be compared with the standard feedback-only control or any other combined Ff/Fb structure where the feedback controller C_b also affects the nominal tracking performance of the system. Furthermore, the results in [30] and [31] quantify, in terms of distance metrics and stability margins, how the nominal stability margin, the nominal tracking transfer function $T_{\mathrm{ry}} = NF$, and the nominal control action $T_{\mathrm{ru}} = MF$ change when there is a discrepancy between the real plant and the nominal plant used in design.

Another control architecture is proposed in [30] to eliminate the detrimental effects of feedback control on tracking performance. In that structure, the feedback controller C_b is decomposed into a left coprime factorization $C_b = \tilde{V}^{-1}\tilde{U}$ with $\tilde{V}$ and $\tilde{U}$ satisfying the Bezout identity $\tilde{V}M + \tilde{U}N = I$. The designed controller is then implemented in two parts such that $\tilde{V}^{-1}$ appears in the forward path and $\tilde{U}$ appears in the feedback path. The architecture shown in Fig. 1 from [28] and [29] with $(X, Y) = (M, N)$ is equivalent to the feedback architecture in [30], yet, the advantage as shown in Fig. 1 is that the controller C_b does not need to be split up into two parts. Hence, we focus on the feedback architecture shown in Fig. 1 to propose an enhanced tracking control design for nanopositioning systems and this control architecture will be considered in the rest of the paper.

A. Coprime Factorization Over $\mathcal{RH}_\infty$

It has been shown in the previous subsection that coprime factorization of the open loop system plays a crucial role in shaping the tracking performance of the presented combined Ff/Fb scheme via the design of the reference and feedforward filters such that $Y = N$ and $X = M$. Coprime factorization over $\mathcal{RH}_\infty$ is not unique and in the sequel, the inner–outer factorization and the normalized coprime factorization are discussed as two special forms of coprime factorization that can be successfully used for the design of the Ff/Fb control structure for nanopositioning systems.

B. Inner–Outer Factorization

Inner–outer factorization (iof) is a special case of coprime factorization where for $G \in \mathcal{RH}_\infty$ the inner–outer factorization $G = NM^{-1}$ gives N as an inner factor and M^{-1} as an outer factor. The transfer function N is called inner if $N \in \mathcal{RH}_\infty$ and $N^*N = I$ where the operation $*$ is the $\mathcal{L}_2$-adjoint. If M^{-1} is stable and minimum phase, it is called an outer factor of G. Details on the computation of inner–outer factorization that includes the case of G being a biproper system can be found in [32] and references therein.

The inner–outer factorization is unique up to a constant unitary matrix and it is specifically useful for nonminimum phase but stable nanopositioning systems. The inner–outer factorization for a nonminimum phase stage gives M^{-1} as a minimum phase approximation obtained by reflecting all unstable zeros into their mirrored stable zeros around the imaginary axis. The bandwidth of the output signal is limited only by the locations of the nonminimum phases zeros of N. Using an inner–outer factorization for the discussed Ff/Fb structure has the advantage that the feedforward filter has intuitive frequency domain properties.

C. Normalized Coprime Factorization

A coprime factorization $G = NM^{-1}$ is normalized right coprime factorization over $\mathcal{RH}_\infty$ when (N, M) are right coprime and $N^*N + M^*M = I$. The normalized coprime factorization (ncf) is unique up to right multiplication by a unitary matrix. The definition of the normalized coprime factorization means that $\begin{bmatrix} N \\ M \end{bmatrix}$ is inner. This inner property induces that if the nanopositioning system G has high-gain at low frequencies, then N has a gain close to unity and M is small at low frequencies. Similarly, if G has small-gain at high frequencies, then N is small and M is close to unity at high frequencies [33]. Therefore, considering the control structure shown in Fig. 1 and for good tracking design, the frequency response of the nanopositioning system has to be shaped first using pre- and postweight functions W_1 and W_2, and then the normalized coprime factorization can be obtained for the shaped system[1] $G_s = N_s M_s^{-1} = W_2 G W_1$. Using this technique, the weights W_1 and W_2 need to be included in the design structure directly and the architecture becomes as shown in Fig. 2. In this case, the reference-to-output and reference-to-input functions become, respectively, $T_{\mathrm{ry}} = W_2^{-1} N_s F$ and $T_{\mathrm{ru}} = W_1 M_s F$.

---

[1]In general, multiaxis nanopositioning systems can be assumed symmetric and have sufficiently small gain at high frequencies to reject noise. Hence, we can put $W_2 = I$ and the frequency response can be shaped using W_1 only.
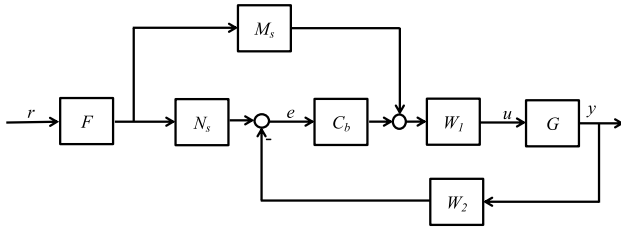
Fig. 2.   Equivalent control structure using normalized coprime factorization for a shaped frequency response of the nanopositioning stage model. The frequency response is shaped using the weights W_1 and W_2.

III. APPLICATION: THE NANOPOSITIONING SYSTEM NPS-XY-100 A

This section presents a case study for the design and implementation of the proposed Ff/Fb control structure. The commercial nanopositioning stage NPS-XY-100A from Queensgate, Inc. is considered as an example. The model of the stage is identified first, and then the controller is designed and implemented in hardware setup.

A. System Identification

The NPS-XY-100A stage is a nanopositioning system of two axes, x and y, with piezoelectric actuators and capacitive sensors. The supplied input to the system, u_x and u_y, are the voltages for the piezoelectric actuators, and the outputs, y_x and y_y, are the displacement along the two perpendicular axes represented by the voltage measured from the capacitive sensors. The stage is driven by two independent electronic circuitry units (NPS2100). To obtain the MIMO (two-by-two) model of the stage over the frequency range of interest, a pseudorandom binary sequence (PRBS) signal of 0.4 V_{pp} (peak-to-peak magnitude) is applied to each input independently and the outputs of both channels are measured. The signal is applied to the system and the output is measured via the National Instruments DAQ card NI PCI-6154 with a sampling rate of 10 kHz. The signals are processed and the model is obtained using the subspace method via MATLAB System Identification Toolbox.

The measured response of the stage shows a symmetrical structure with near identical frequency response of both channels x and y. In addition, the frequency response indicates a nonminimum phase lightly damped system with multimode resonance frequency. The first resonant peak, identical for both channels xx and yy, occurs in the region of 1–1.5 krad/s with a dynamic range of about 10 dB. Fig. 3 shows the frequency response of the stage[2] along with the fitted continuous time transfer function for the diagonal channels G_{xx} and G_{yy}. The fitted transfer function is biproper of order 30 and achieves a fitting accuracy of 96.21% to collected data with MSE of 2.123×10^{-5}. Making the fitted model a biproper transfer function is to minimize the effect of the modes corresponding to frequencies that lie outside the frequency region of interest [34].

[2]For simplicity of representation, all phase graphs in this paper have the phase response wrapped to be in the range $[-180°, 180°]$.
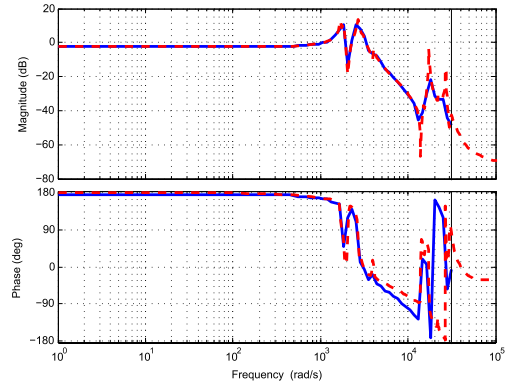
Fig. 3.   Measured frequency response. Solid line: of the open-loop diagonal channels . Dashed line: of the fitted transfer function. The response is identical for both channels xx and yy.
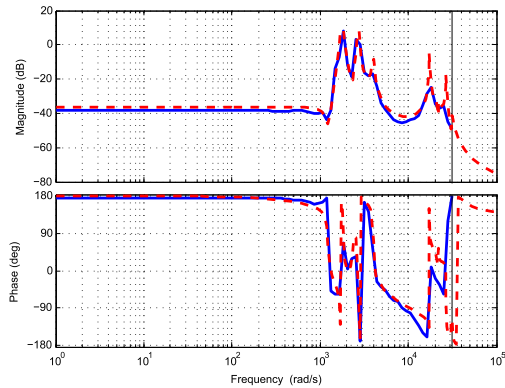
Fig. 4.   Measured frequency response. Solid line: of the open loop cross-coupling channels. Dashed line: of the fitted transfer function. The response is identical for both channels, xy and yx.
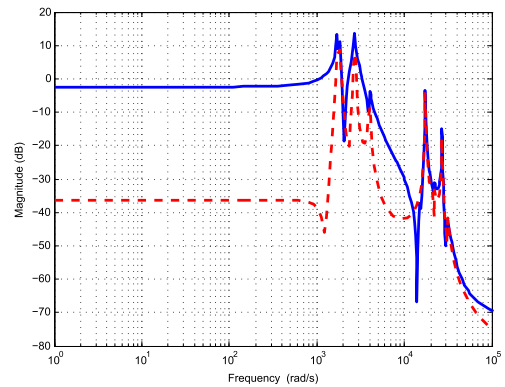
Fig. 5.   Magnitude of frequency response. Solid line: for the diagonal channels. Dashed line: for the cross-coupling channels.

Fig. 4 shows the coupling frequency response and the continuous time fitted transfer function for both channels G_{xy} and G_{yx}, which is identical in both directions. The fitted transfer function is of order 20 and achieves a fitting accuracy of 95.64% to collected data with MSE of 5.983×10^{-06}. The cross-coupling gain between the two channels is small at low frequency. However, as the frequency increases, the cross-coupling becomes higher (Fig. 5). Therefore, for high bandwidth, which is the design target of this paper, a MIMO model of the stage is needed.
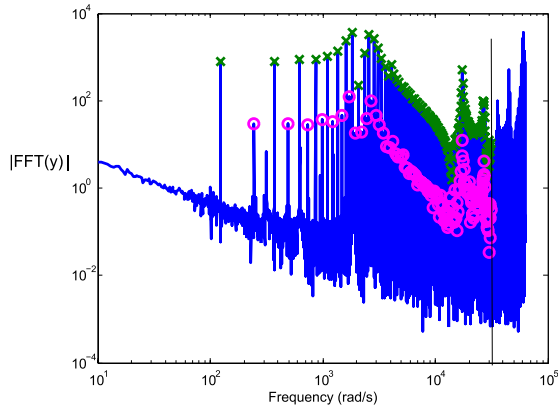
Fig. 6. Output spectrum of response of the excited channel: the response at excited frequencies is marked by crosses and circles indicate nonlinearity since excitation at even harmonics is suppressed.

Fig. 7. Singular values plot. Solid line: nominal stage model G. Dashed line: shaped system G_s.

The nonlinearity of the stage can be captured by plotting the Fourier Transform of the system response as shown in Fig. 6. The PRBS signal has a length of 255 samples repeated n times to cover the length time of the experiment, with n being an even number. Every other term is inverted so that the even harmonics are suppressed [35]. The relative excitation at these frequencies then indicates the level of nonlinearity (Fig. 6). Although nonlinearities are present and the main cause for these nonlinearities can be related to hysteresis [1], the linear response is seen to dominate for the frequency range of interest and hence the system is assumed linear. This matches the manufacturing specifications of the stage that states a maximum linearity error of 0.02%, which equals to an error of 0.02 μm for the total range of 100 μm of the stage.

B. Nonminimum Phase Zeros

Generally speaking, the nonminimum phase zeros in nanopositioning models arise at high frequencies and are most likely due to delay in the actuator/sensor electronics. The fitted real-rational model approximates this delay with a Padé type approximation, thereby introducing nonminimum phase zeros at high frequencies. The delay in nanopositioning systems can arise from several factors such as sampling delay, noncollocated geometry of the stage's sensors and actuators, low bandwidth of the voltage amplifiers that drive the circuits or the low bandwidth of position sensors of the stage. In our case, the reader should note that the measured frequency response of the system includes the dynamics of all driving electronic units, the data acquisition card, and its driving PC that exist in the loop. The measured delay is four samples which equals to 0.4 ms. The HV amplifier and the NanoSensor of the controller unit (NPS2110) have bandwidths of 10 and 5 kHz, respectively. These two bandwidths are not high enough and could cause a delay in the measured response of the stage in the frequency region of interest. Therefore, the nonminimum phase zeros of the frequency response can be interpreted in light of the nondisclosed geometry of the stage and the existence of extra electronic circuitry with limited bandwidth in the loop. This information is important when interpreting the phase response of the system shown in Figs. 3 and 4.
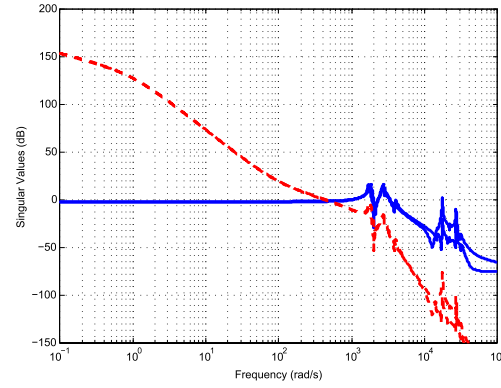
C. Feedback Control

We design the feedback control C_b by using the $\mathscr{H}_\infty$ loop shaping design method as proposed in [33]. Justification for the suitability of the $\mathscr{H}_\infty$ loop shaping control design and its robustness properties for nanopositioning stages can be found in [7] and [25]. In a standard $\mathscr{H}_\infty$ loop shaping control design, the precompensator W_1 and postcompensator W_2 are chosen to give the nominal plant G the desired frequency response for performance design. Then, after shaping the open loop system, a controller K_∞ is synthesized to stabilize the shaped system $G_s = W_2 G W_1$ and to maximize the robust stability margin. The design of weighting functions in $\mathscr{H}_\infty$ loopshaping is not difficult and can be done by hand or using optimization software [36]. The feedback controller C_b needs to be designed as best as possible using standard robustness design criteria regardless of the filters X and Y.

As the stage is symmetric and has sufficient rolloff rate at high frequency, we put $W_2 = I$ and the precompensator weight W_1 is chosen to give the nominal stage model G the desired frequency response to achieve maximum bandwidth and 0% steady-state error while maintaining a good stability margin. Fig. 7 shows the singular values of the nominal stage model G and the open loop shaped system G_s where the designed shaping weight is $W_1 = 6 \times 10^8 (s + 100)^2 / s(s + 1)^2 (s + 1000)^2$. The achieved stability margin is 0.38 which represents an allowance for normalized coprime factors uncertainty of 38%.

The implementation of the feedback controller depends on the chosen coprime factorization to design the reference and feedforward filters. For instance, if the normalized coprime factorization is to be used, then the implemented controller is $C_b^{\mathrm{ncf}} = K_\infty$, and the weights W_1 and W_2 are implemented directly in the loop as shown in Fig. 2 with $Y = N_s$ and $X = M_s$ where $G_s = W_2 G W_1 = N_s M_s^{-1}$. For the choice of inner–outer factorization, the implemented controller is the total function $C_b^{\mathrm{iof}} = W_1 K_\infty W_2$ and its singular values plot is shown in Fig. 8. In this case, the structure is implemented in standard form as shown in Fig. 1 with $Y = N$ and $X = M$ where $G = N M^{-1}$. We choose to absorb the weights with the controller in this case so that the feedforward injection is at the plant input as is common in the literature. Thus our results can be compared with published results. Note, however, that
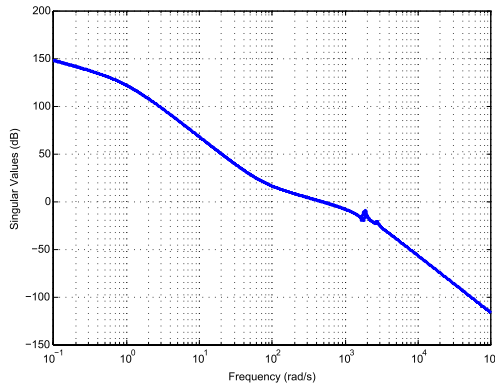
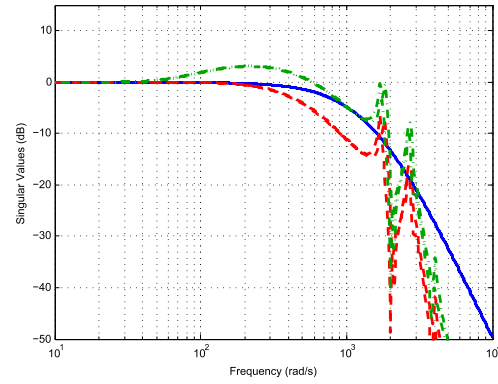Fig. 8.   Singular vales plot of the designed MIMO feedback controller $C_b^{iof} = W_1 K_\infty W_2$.

Fig. 9.   Singular values plots of the designed closed-loop reference-to-output tracking transfer function T_{ry}. Three control designs: Ff/Fb associated with iof (blue solid line), Ff/Fb associated with ncf (red dashed line), and feedback-only control (green dash-dotted line).
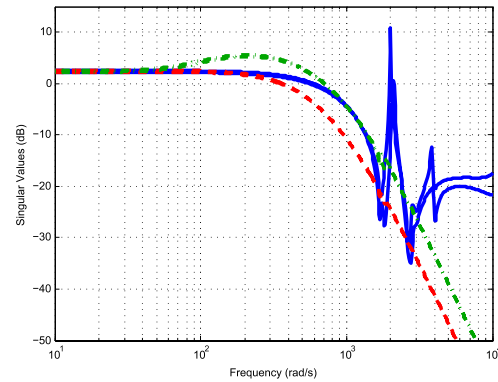

Fig. 10.   Singular values plots of the designed closed-loop reference-to-input transfer function T_{ru}. Three control designs: Ff/Fb associated with iof (blue solid line), Ff/Fb associated with ncf (red dashed line), and feedback-only control (green dash-dotted line).

the injection could still take place before the weight W_1 as shown in Fig. 2 if one wishes.

D. Reference and Feedforward Filters

The reference and feedforward filters are designed using both choices of coprime factorization discussed before, that is, inner–outer factorization (iof) and normalized coprime factorization (ncf).

For the case of inner-outer factorization, both factors N and M include high-frequency gain. However, for practical reasons, the design requires a limited bandwidth to avoid actuator saturation, undesirable saturation, and so forth. Hence, the initial reference filter F should be designed as a low-pass filter $F = 1/(s/\alpha + 1)^\beta I$ where I is an identity matrix of suitable dimension. The parameter $\beta \geq 1$ and its value depends on the physical properties of the stage such as saturation limit and skew rate of the actuators. The parameter $\alpha > 0$ and its value is determined by the required bandwidth of the system. In our case, we choose $\alpha = 1500$ rad/s and $\beta = 3$. Using this design and for the nominal case, the reference-to-output and reference-to-input transfer functions become, respectively, $T_{ry}^{iof} = NF$ and $T_{ru}^{iof} = MF$.

For the choice of normalized coprime factorization, the design of the reference and feedforward filters is dictated by the normalized right coprime factorization of the shaped system used for the feedback controller synthesis in the previous subsection. Hence, the reference and feedforward filters are designed such as $X^{ncf} = M_s$ and $Y^{ncf} = N_s$, respectively. Putting $F = I$ and using this design, the reference-to-output and reference-to-input transfer functions in the nominal case become $T_{ry}^{ncf} = N_s$ and $T_{ru}^{ncf} = W_1 M_s$.

For comparison analysis, Fig. 9 shows the singular values plots of the designed tracking transfer function when using both coprime factorizations, iof and ncf, for the design of the reference and feedforward filters. The tracking transfer function for the case of feedback-only control (i.e., $X = 0$, $Y = F = I$) is also included to clarify the merits of the proposed combined Ff/Fb structure. This figure highlights the benefits of the Ff/Fb structure contrasted with the feedback-only control where the nominal tracking performance of the system is decoupled completely from the feedback controller in case of the Ff/Fb control design. This can be seen from

the damped peak in the frequency response of the closed-loop system that exists only in the case of the feedback-only control. This peak corresponds to an overshoot in the closed-loop time-domain response. The inner–outer factorization produces a higher bandwidth and nominally the system can be operated at bandwidth higher than the first resonant peak. However, the robustness of the system is limited by the bandwidth of the feedback controller. This means any achieved nominal tracking bandwidth beyond the bandwidth of the feedback controller will be highly susceptible to noise and model uncertainty. For the case of the normalized coprime factorization, the nominal tracking transfer function is automatically associated with the robust performance guarantees of the feedback loop when the feedback controller is chosen via $\mathcal{H}_\infty$ loop shaping. The proposed Ff/Fb structure associated with ncf achieves a bandwidth of 421.94 rad/s with 0% overshoot while maintaining the robustness guarantees of the feedback control. Guaranteeing 0% overshoot by a feedback-only control, the maximum bandwidth that was obtained by the authors was only 60.34 rad/s.

In Fig. 10, the singular values plots of the designed reference-to-input transfer functions for the three control designs (Ff/Fb with ncf, Ff/Fb with iof and feedback-only control) are presented. This figure can be used as a measure for
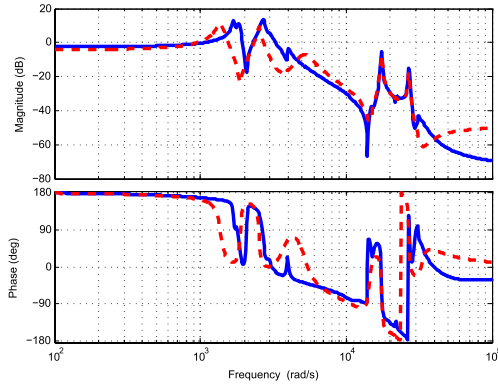
Fig. 11. Frequency response of the open loop diagonal channels. Solid line: case with no-load. Dashed line: case with 800 g load.

the control effort needed in each case to achieve the nominal tracking performance of the system. The figure shows that for high-frequency input commands, the Ff/Fb associated with iof contains undesirable resonance peaks which makes the system prone to actuator saturation and high control action due to noise and model uncertainty. The case of the feedback-only control has a small damped peak before the transfer function rolls off in high frequencies. This peak does not exist for the Ff/Fb structure with ncf which is advantageous to avoid actuator saturation for command signals operating at the same frequency region.

E. No-Load Stage Versus Loaded Stage

One of the major challenges in controlling nanopositioning stages is the performance of these systems under load variations, that is, not in the nominal case. This is due to the structure and dynamics of these systems where the response of the stage changes dramatically following changes in load. For instance, in AFM applications the load of the stage is a representation of the weight of the sample to be scanned. For the stage in hand, the maximum allowed load weight is 1000 g. Fig. 11 shows the open loop model of the diagonal channels, $G_{xx} = G_{yy}$, of the stage for the nominal case of no-load and under the load of 800 g. The model of the stage under the load is identified using the same procedure presented before for identifying the no-load model. It can be seen that for the loaded case, the locations of the poles change and the resonant peaks of the frequency response shifts to the left. This is a well understood phenomenon of flexible structures which induces significant unstructured uncertainty [3], [30], [31], and it makes the problem very challenging. Hence, the purpose of the control system for nanopositioning stages is to guarantee robust stability and robust tracking performance under load variations. Fig. 12 shows the singular values plots of the closed-loop reference-to-output tracking transfer function T_{ry} for the no-load case and under the load of 800 g with the control structure being: Ff/Fb associated with iof, Ff/Fb associated with ncf and feedback-only control, respectively. It can be seen that the Ff/Fb associated with ncf is superior over the other designs with less deterioration in the tracking performance. This can be interpreted in light of the properties of normalized

coprime factorization of shaped systems (see [30], [31], [33] for more details). Stability robustness of the system under load variations is guaranteed by the designed $\mathscr{H}_\infty$ feedback controller for all three control designs.

Therefore, it can be seen from Figs. 9, 10, and 12 that the proposed Ff/fb control structure associated with ncf produces the best tracking performance with high bandwidth and robustness to load variations. The Ff/Fb associated with iof can be used to obtain high bandwidth but at the expense of high control action which could be highly susceptible to noise and model uncertainty. It is also less robust to load variations. For the case study presented in this paper, the normalized coprime factorization is considered and the experimental results presented next are for the combined Ff/Fb control scheme by using normalized coprime factorization as shown in the block diagram in Fig. 2.

F. Noise Responses

Following the discussion of [37], three main sources of noise affect the positioning resolution of nanopositioning systems: amplifier voltage noise d_i, external noise d_o, and sensor noise n. As shown in Fig. 1, the transfer functions from these noise sources to the position of the stage are given respectively by

$$T_{d_i y} = (I + C_b G)^{-1} G \qquad (3)$$

$$T_{d_o y} = (I + C_b G)^{-1} \qquad (4)$$

$$T_{ny} = -(I + C_b G)^{-1} C_b G. \qquad (5)$$

From (3)–(5), it can be seen that the noise responses depend only on the feedback controller and indeed neither the feedforward nor the reference filters appear in these transfer functions. Hence, for the proposed Ff/Fb control design, the choice of the reference and feedforward filters X and Y does not affect the robustness against noises in the closed-loop system.

G. Experimental Results

The designed control scheme is implemented to control the NPS-XY-100A stage by using LabView RT module. The update rate of the controller is 8 kHz and the response is measured using the NI DAQ card NI PCI-6154 with 8 kHz sampling frequency. Fig. 13 shows the system setup for the experiment.

To demonstrate the merits of the proposed Ff/Fb control structure, the results in this section are presented for the closed loop with two control designs: feedback-only control and the proposed Ff/Fb associated with ncf. The case of the feedback-only control indicates the same feedback controller used in the Ff/Fb design with $X = 0$ and $F = Y = I$.

1) No-Load Case: The experimental frequency responses of the no-load closed-loop transfer functions T_{ry} and T_{ru} for both control designs are shown in Figs. 14 and 15, respectively. The graphs show the superiority of the proposed control scheme over the feedback-only control where the frequency response of the tracking transfer function of the latter indicates a 5 dB damped peak that represents more than 20% overshoot. Moreover, the reference-to-input transfer function for the case
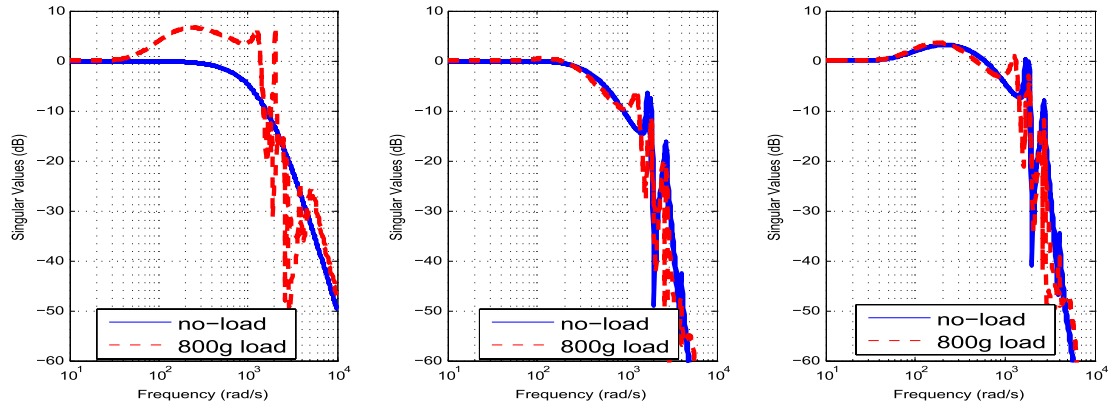
Fig. 12. Singular values plots of the designed closed-loop tracking transfer function T_{ry}. Three control designs: Ff/Fb associated with iof (left), Ff/Fb associated with ncf (middle), and feedback-only control (right). For each design, two cases are considered: (solid line) the no-load case and (dashed line) the 800 g load case.
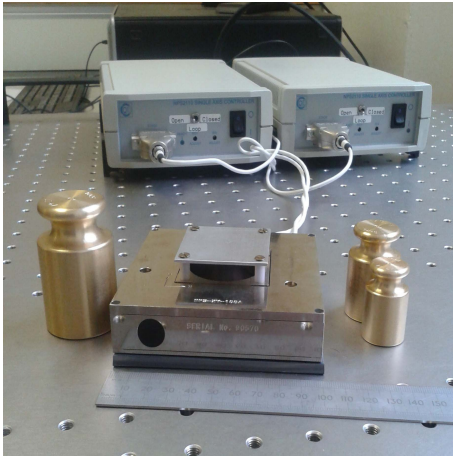

Fig. 13. Experimental hardware setup for controlling the NPS-XY-100A nanopositioning stage. The stage with the load adapter beside three load masses: 100 g, 200 g, and 500 g (front). The two NPS2100 NanoSensor single channel standalone modules (back).
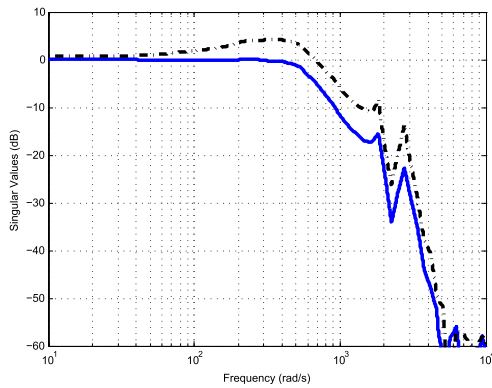
Fig. 14. Experimental frequency response of the closed-loop reference-to-output tracking transfer function T_{ry} for the nominal case with no load on the stage. Two control designs are considered: (solid line) Ff/Fb associated with ncf and (dashed line) feedback-only control.

of the feedback-only control has also a peaked region which indicates higher input energy to the stage in comparison with the case of the proposed control architecture for a reference signal in this frequency region.
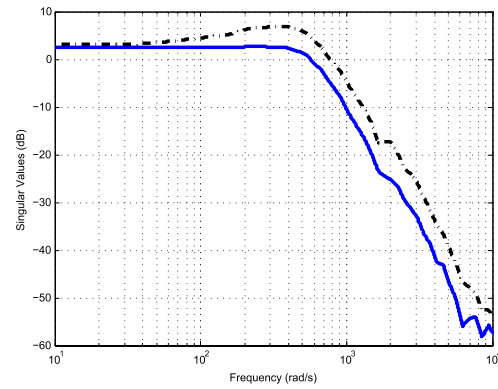
Fig. 15. Experimental frequency response of the closed-loop reference-to-input transfer function T_{ru} for the nominal case with no load on the stage. Two control designs are considered: (solid line) Ff/Fb associated with ncf and (dashed line) feedback-only control.

Figs. 16 and 17 show the time domain closed-loop response of the system to a reference signal on x channel for the case of feedback-only control and Ff/Fb with ncf, respectively. Two reference signals of 1 V_{pp} triangular wave and two frequencies, 15 and 30 Hz, are injected to the system. The graphs show good tracking of the reference signal when using the proposed Ff/Fb control architecture and confirm the overshoot in the case of the feedback-only control design. The stage is inverted which explains the phase shift between the reference and input signals (see the phase plot shown in Fig. 3 for details).

2) Loaded Case: A mass of 800 g is used to load the stage and the response of the closed-loop system is replotted under the same reference signals used before in the no-load case, that is, a triangular wave of 1 V_{pp} magnitude and two frequencies: 15 and 30 Hz. The closed-loop experimental reference-to-output tracking transfer function T_{ry} and the reference-to-input transfer function T_{ru} for the case of the loaded stage with 800 g mass and two nominal control designs, Ff/Fb associated with ncf and feedback-only control, are shown in Figs. 18 and 19, respectively. The system follows the command signal with a good accuracy when the proposed Ff/Fb with ncf control scheme is used as shown in Fig. 21. This is to be compared with the response of the system for the case of feedback-only control as shown in Fig. 20. It can be seen from these
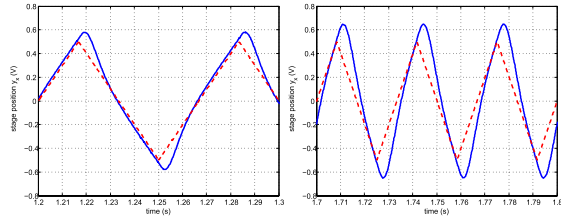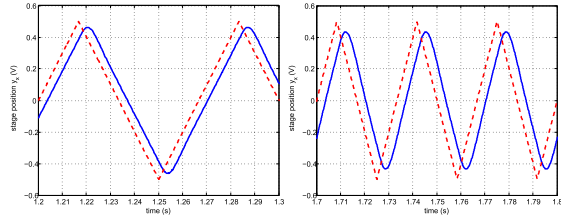
(a) The output signal of the stage (solid line) in response to the reference signal (dashed line).
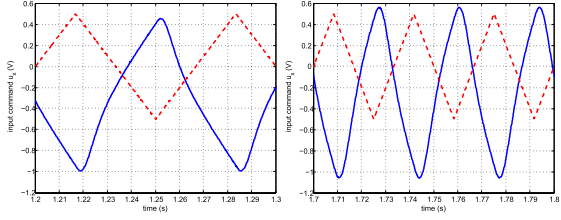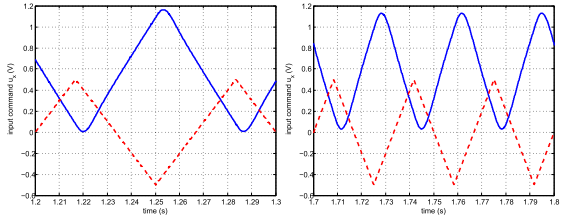

(b) The input signal to the stage (solid line) in response to the reference signal (dashed line).

Fig. 16.   x-channel closed-loop output and input signals in response to a triangular wave reference signal of 1 V_{pp} magnitude and two frequencies: (left) 15 Hz and (right) 30 Hz; experimental data for the case of no-load on the stage and feedback-only control. (a) Output signal of the stage (solid line) in response to the reference signal (dashed line). (b) Input signal to the stage (solid line) in response to the reference signal (dashed line).

(a) The output signal of the stage (solid line) in response to the reference signal (dashed line).

(b) The input signal to the stage (solid line) in response to the reference signal (dashed line).

Fig. 17.   x-channel closed loop output and input signals in response to a triangular wave reference signal of 1 V_{pp} magnitude and two frequencies: (left) 15 Hz and (right) 30 Hz; experimental data for the case of no-load on the stage and Ff/Fb associated with ncf. (a) Output signal of the stage (solid line) in response to the reference signal (dashed line). (b) Input signal to the stage (solid line) in response to the reference signal (dashed line).

graphs that there is less deterioration in the response under the proposed Ff/Fb control scheme.

To quantify the improvement on the tracking for the proposed control structure over the feedback-only control, Table I summarizes the maximum positioning error of the closed-loop system for the two control designs. The table includes the no-load case and the loaded case with different loads on the stage and various frequencies of the triangular wave reference signal. The table shows that the proposed control architecture produces the smallest worst case error across all loads and frequencies. Furthermore, to demonstrate the enhancement of the proposed control system graphically, Fig. 22 shows the positioning error between the reference
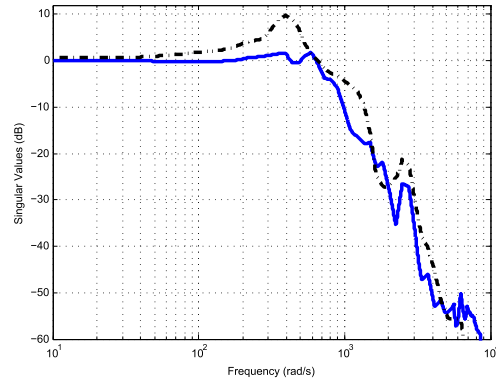

Fig. 18.   Experimental frequency response of the closed-loop reference-to-output tracking transfer function T_{ry} for the case of 800 g load on the stage. Two control designs are considered: (solid line) Ff/Fb associated with ncf and (dashed line) feedback-only control.
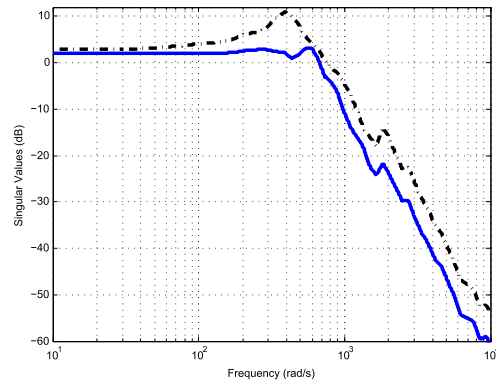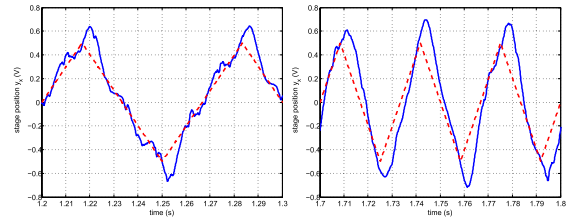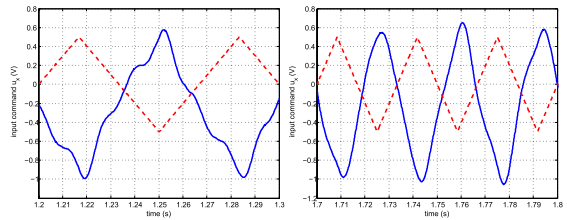

Fig. 19.   Experimental frequency response of the closed-loop reference-to-input transfer function T_{ru} for the case of 800 g load on the stage. Two control designs are considered: (solid line) Ff/Fb associated with ncf and (dashed line) feedback-only control.

(a) The output signal of the stage (solid line) in response to the reference signal (dashed line).

(b) The input signal to the stage (solid line) in response to the reference signal (dashed line).

Fig. 20.   x-channel closed-loop output and input signals in response to a triangular wave reference signal of 1 V_{pp} magnitude and two frequencies: (left) 15 Hz and (right) 30 Hz; experimental data for the case of 800 g load on the stage and feedback-only control. (a) Output signal of the stage (solid line) in response to the reference signal (dashed line). (b) Input signal to the stage (solid line) in response to the reference signal (dashed line).

signal and the actual position of the stage for a chosen reference signal of 30 Hz frequency. Two cases are considered; the no-load case and the case of 800 g loading.
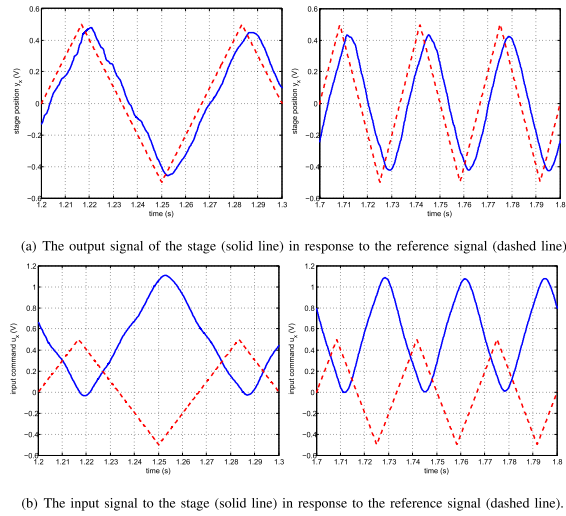
(a) The output signal of the stage (solid line) in response to the reference signal (dashed line).

(b) The input signal to the stage (solid line) in response to the reference signal (dashed line).

Fig. 21.   x-channel closed-loop output and input signals in response to a triangular wave reference signal of 1 V_{pp} magnitude and two frequencies: (left) 15 Hz and (right) 30 Hz; experimental data for the case of 800 g load on the stage and Ff/Fb associated with ncf. (a) Output signal of the stage (solid line) in response to the reference signal (dashed line). (b) Input signal to the stage (solid line) in response to the reference signal (dashed line).

TABLE I

CLOSED-LOOP MAXIMUM POSITIONING ERROR OF THE STAGE POSITION UNDER VARIOUS REFERENCE SIGNALS AND LOADS ON THE STAGE. TWO CONTROL DESIGNS ARE CONSIDERED: Ff/Fb WITH ncf AND FEEDBACK-ONLY CONTROL

load and reference frequency	Maximum positioning error (V)	
	Ff/Fb with ncf	feedback-only
no load, 15 Hz	0.1353	0.1869
no load, 30 Hz	0.2490	0.3562
100 g, 15 Hz	0.1234	0.1857
100 g, 30 Hz	0.2469	0.3578
500 g, 15 Hz	0.1842	0.2573
500 g, 30 Hz	0.2857	0.4091
800 g, 15 Hz	0.1626	0.2641
800 g, 30 Hz	0.2664	0.4255

(a) No-load case   (b) Loaded stage with 800 g
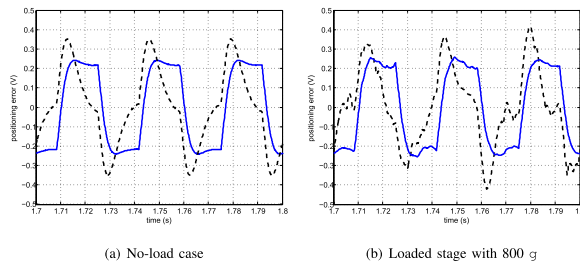
Fig. 22.   Positioning error for the cases of Ff/Fb with ncf (solid line) and feedback-only control (dashed line) in response to a triangular reference signal of 30 Hz and 1 V_{pp} magnitude. (a) Nominal case with no load. (b) Loaded stage with 800 g.

IV. CONCLUSION

Using a special form of combined feedforward/feedback control structure as shown in Fig. 1, good tracking performance properties and good robustness properties can be achieved for nanopositioning systems. In this control architecture, the tracking performance of the loop is inde-

pendent of the feedback controller in the nominal case. Furthermore, the nominal control signal is independent of the feedback controller. Therefore, the nominal tracking performance criteria can be designed independently from the feedback controller which should be designed for robustness and noise reduction. Two forms of coprime factorization are discussed for the design of the reference and feedforward filters; the inner–outer factorization and the normalized coprime factorization. As a case study, the control scheme is applied to the commercial nanostage NPS-XY-100A from Queensgate using normalized coprime factorization. The proposed control achieves a bandwidth of 25% of the natural frequency of the first resonant peak and exhibits robustness against load variation on the stage. Results are verified in an experimental study using a triangle reference input of different frequencies.

REFERENCES

[1] S. Devasia, E. Eleftheriou, and S. O. R. Moheimani, "A survey of control issues in nanopositioning," *IEEE Trans. Control Syst. Technol.*, vol. 15, no. 5, pp. 802–823, Sep. 2007.
[2] J. A. Main and E. Garcia, "Piezoelectric stack actuators and control system design: Strategies and pitfalls," *J. Guid., Control, Dyn.*, vol. 20, no. 3, pp. 479–485, 1997.
[3] A. J. Fleming, "Nanopositioning system with force feedback for high-performance tracking and vibration control," *IEEE/ASME Trans. Mechatronics*, vol. 15, no. 3, pp. 433–447, Jun. 2010.
[4] D. Croft, G. Shedd, and S. Devasia, "Creep, hysteresis, and vibration compensation for piezoactuators: Atomic force microscopy application," in *Proc. Amer. Control Conf.*, vol. 3. 2000, pp. 2123–2128.
[5] A. Lanzon and I. R. Petersen, "Stability robustness of a feedback interconnection of systems with negative imaginary frequency response," *IEEE Trans. Autom. Control*, vol. 53, no. 4, pp. 1042–1046, May 2008.
[6] M. A. Mabrok, A. G. Kallapur, I. R. Petersen, and A. Lanzon, "Spectral conditions for negative imaginary systems with applications to nanopositioning," *IEEE/ASME Trans. Mechatronics*, vol. 19, no. 3, pp. 895–903, Jun. 2014.
[7] S. Salapaka, A. Sebastian, J. P. Cleveland, and M. V. Salapaka, "High bandwidth nano-positioner: A robust control approach," *Rev. Sci. Instrum.*, vol. 73, no. 9, pp. 3232–3241, Sep. 2002.
[8] G. M. Clayton, S. Tien, K. K. Leang, Q. Zou, and S. Devasia, "A review of feedforward control approaches in nanopositioning for high-speed SPM," *J. Dyn. Syst., Meas., Control*, vol. 131, no. 6, pp. 061101-1–061101-19, 2009.
[9] S. S. Aphale, A. J. Fleming, and S. O. R. Moheimani, "Integral resonant control of collocated smart structures," *Smart Mater. Struct.*, vol. 16, no. 2, pp. 439–446, 2007.
[10] B. Potsaid and J. T. Wen, "High performance motion tracking control," in *Proc. IEEE Int. Conf. Control Appl.*, vol. 1. Sep. 2004, pp. 718–723.
[11] M. W. Fairbairn, S. O. R. Moheimani, and A. J. Fleming, "*Q* control of an atomic force microscope microcantilever: A sensorless approach," *J. Microelectromech. Syst.*, vol. 20, no. 6, pp. 1372–1381, Dec. 2011.
[12] S. K. Das, O. U. Rehman, H. R. Pota, and I. R. Petersen, "Minimax LQG controller design for nanopositioners," in *Proc. 13th Eur. Control Conf. (ECC)*, Jun. 2014, pp. 1933–1938.
[13] J. C. Doyle, B. A. Francis, and A. R. Tannenbaum, *Feedback Control Theory*. New York, NY, USA: Dover, 2009.
[14] A. A. Eielsen, M. Vagia, J. T. Gravdahl, and K. Y. Pettersen, "Damping and tracking control schemes for nanopositioning," *IEEE/ASME Trans. Mechatronics*, vol. 19, no. 2, pp. 432–444, Apr. 2014.

[15] D. Croft and S. Devasia, "Vibration compensation for high speed scanning tunneling microscopy," *Rev. Sci. Instrum.*, vol. 70, no. 12, pp. 4600–4605, Dec. 1999.

[16] G. Schitter, P. J. Thurner, and P. K. Hansma, "Design and input-shaping control of a novel scanner for high-speed atomic force microscopy," *Mechatronics*, vol. 18, nos. 5–6, pp. 282–288, 2008.

[17] S. Devasia, "Should model-based inverse inputs be used as feedforward under plant uncertainty?" *IEEE Trans. Autom. Control*, vol. 47, no. 11, pp. 1865–1871, Nov. 2002.

[18] K. J. Åström and R. M. Murray, *Feedback Systems: An Introduction for Scientists and Engineers*. Princeton, NJ, USA: Princeton Univ. Press, 2008.

[19] M. Iwasaki, K. Seki, and Y. Maeda, "High-precision motion control techniques: A promising approach to improving motion performance," *IEEE Ind. Electron. Mag.*, vol. 6, no. 1, pp. 32–40, Mar. 2012.

[20] K. Seki, Y. Tsuchimoto, and M. Iwasaki, "Feedforward compensation by specified step settling with frequency shaping of position reference," *IEEE Trans. Ind. Electron.*, vol. 61, no. 3, pp. 1552–1561, Mar. 2014.

[21] J. A. Butterworth, L. Y. Pao, and D. Y. Abramovitch, "A comparison of control architectures for atomic force microscopes," *Asian J. Control*, vol. 11, no. 2, pp. 175–181, 2009.

[22] E. Eleftheriou and S. O. R. Moheimani, Eds., *Control Technologies for Emerging Micro and Nanoscale Systems* (Lecture Notes in Control and Information Sciences), vol. 413. New York, NY, USA: Springer-Verlag, 2011, ch. 4.

[23] L. Y. Pao, J. A. Butterworth, and D. Y. Abramovitch, "Combined feedforward/feedback control of atomic force microscopes," in *Proc. Amer. Control Conf.*, Jul. 2007, pp. 3509–3515.

[24] Y. K. Yong, S. S. Aphale, and S. O. R. Moheimani, "Design, identification, and control of a flexure-based XY stage for fast nanoscale positioning," *IEEE Trans. Nanotechnol.*, vol. 8, no. 1, pp. 46–54, Jan. 2009.

[25] A. Sebastian and S. M. Salapaka, "Design methodologies for robust nano-positioning," *IEEE Trans. Control Syst. Technol.*, vol. 13, no. 6, pp. 868–876, Nov. 2005.

[26] Y. K. Yong, K. Liu, and S. O. R. Moheimani, "Reducing cross-coupling in a compliant XY nanopositioner for fast and accurate raster scanning," *IEEE Trans. Control Syst. Technol.*, vol. 18, no. 5, pp. 1172–1179, Sep. 2010.

[27] M. Vidyasagar, *Control System Synthesis: A Factorization Approach* (Synthesis Lectures on Control and Mechatronics). San Rafael, CA, USA: Morgan & Claypool, 2011.

[28] A. Lanzon, A. Lecchini, A. Dehghani, and B. D. O. Anderson, "Checking if controllers are stabilizing using closed-loop data," in *Proc. 45th IEEE Conf. Decision Control*, Dec. 2006, pp. 3660–3665.

[29] A. Dehghani, A. Lecchini-Visintini, A. Lanzon, and B. D. O. Anderson, "Validating controllers for internal stability utilizing closed-loop data," *IEEE Trans. Autom. Control*, vol. 54, no. 11, pp. 2719–2725, Nov. 2009.

[30] G. Vinnicombe, *Uncertainty and Feedback: H_∞ Loop-Shaping and the ν-Gap Metric*. Singapore: World Scientific, 2001.

[31] A. Lanzon and G. Papageorgiou, "Distance measures for uncertain linear systems: A general theory," *IEEE Trans. Autom. Control*, vol. 54, no. 7, pp. 1532–1547, Jul. 2009.

[32] A. Varga, "Computation of inner-outer factorization of rational matrices," *IEEE Trans. Autom. Control*, vol. 43, no. 5, pp. 684–688, May 1998.

[33] D. McFarlane and K. Glover, "A loop-shaping design procedure using H_∞ synthesis," *IEEE Trans. Autom. Control*, vol. 37, no. 6, pp. 759–769, Jun. 1992.

[34] S. O. R. Moheimani and W. P. Heath, "Model correction for a class of spatio-temporal systems," *Automatica*, vol. 38, no. 1, pp. 147–155, Jan. 2002.

[35] K. R. Godfrey, A. H. Tan, H. A. Barker, and B. Chong, "A survey of readily accessible perturbation signals for system identification in the frequency domain," *Control Eng. Pract.*, vol. 13, no. 11, pp. 1391–1402, 2005.

[36] A. Lanzon, "Weight optimisation in H_∞ loop-shaping," *Automatica*, vol. 41, no. 7, pp. 1201–1208, 2005.

[37] A. J. Fleming, "Measuring and predicting resolution in nanopositioning systems," *Mechatronics*, vol. 24, no. 6, pp. 605–618, 2014.

Mohamed Kara-Mohamed received the B.Sc. (Hons.) degree in electrical and electronic engineering from the University of Aleppo, Aleppo, Syria, in 2002, the master's degree in engineering management from the American University of Beirut, Beirut, Lebanon, in 2006, and the M.Sc. degree in advanced control systems and engineering and the Ph.D. degree in control engineering from the University of Manchester, Manchester, U.K., in 2008 and 2012, respectively.

He held academic positions with Coventry University, Coventry, U.K., and the University of Aleppo. He was a Research Associate with the University of Manchester. He was also with the MTN Group. He is currently an Experimental Officer with the Control Systems Centre, School of Electrical and Electronic Engineering, University of Manchester.

William P. Heath received the B.A. degree in mathematics from the University of Cambridge, Cambridge, U.K., in 1987, and the M.Sc. and Ph.D. degrees from the University of Manchester Institute of Science and Technology, Manchester, U.K., in 1989 and 1992, respectively.

He was with Lucas Automotive Ltd., Gillingham, U.K., from 1995 to 1998, and was a Academic Researcher with the University of Newcastle, Newcastle, NSW, Australia, from 1998 to 2004. He is currently a Reader with the University of Manchester, Manchester, where he is also the Head of the Control Systems Centre, School of Electrical and Electronic Engineering. His current research interests include constrained control and system identification.

Alexander Lanzon received the B.Eng. (Hons). degree in electrical and electronic engineering from the University of Malta, Msida, Malta, in 1995, and the M.Phil. degree in control engineering and the Ph.D. degree in control theory from the University of Cambridge, Cambridge, U.K., in 1997 and 2000, respectively.

He held academic positions with the Georgia Institute of Technology, Atlanta, GA, USA, and Australian National University, Canberra, ACT, Australia, before joining the University of Manchester, Manchester, U.K., in 2006. He was with STMicroelectronics Ltd., Kirkop, Malta, Yaskawa Denki Tokyo Ltd., Tokya, Japan, and National ICT Australia Ltd., Canberra. He holds the rank of Chair in Control Engineering with the University of Manchester.

Prof. Lanzon is an Associate Editor of the IEEE TRANSACTIONS ON AUTOMATIC CONTROL, a Subject Editor of the *International Journal of Robust and Nonlinear Control*, and a fellow of the Institute of Mathematics and its Applications, the Institute of Measurement and Control, and the Institution of Engineering and Technology.